Journal of CO2 Utilization 78 (2023) 102629

Contents lists available at ScienceDirect

Journal of CO2 Utilization

journal homepage: www.elsevier.com/locate/jcou

Modified polyethyleneimine as additive for enhanced direct air capture via membrane contactors

Alireza Zare [a], Ahmed Khatib Boukalfa [a], Adrianna Nogalska [b], Alberto Puga [a], Pierfrancesco Cerruti [c], Borja Pascual-Jose [d], Amparo Ribes-Greus [d], Marta Giamberini [a,*]

[a] Department of Chemical Engineering, Universitat Rovira I Virgili, Av. Països Catalans, 26, 43007 Tarragona, Spain
[b] Eurecat, Centre Tecnològic de Catalunya, C/Marcellí Domingo 2, 43007 Tarragona, Spain
[c] Institute of Polymers, Composites and Biomaterials, National Research Council, Via Campi Flegrei 34, 80078 Pozzuoli, Italy
[d] Institute of Technology of Materials (ITM), Universitat Politècnica de València (UPV), Camí de Vera, s/n, 46022 Valencia, Spain

ARTICLE INFO

Keywords:
Carbon dioxide
Direct air capture
Polyethylene imine
Polysulfone
Phenyl isocyanate
Membrane contactor

ABSTRACT

This paper reports the preparation and characterization of asymmetric membranes for direct air capture (DAC) in polysulfone membrane contactors. In the previous studies it was found that blending the polysulfone with modified Lupasol G20 improved the polysulfone membrane performance; however, the hydrophobicity and stability of the additive require improvement for the application in gas/liquid system. In order to achieve this objective, in the current study, Lupasol G20 was grafted with phenyl isocyanate via urea linkages in a solvent-free and eco-friendly method. Membranes with different amount of the additive were prepared by phase inversion and characterized by several techniques in terms of morphology, porosity, wettability, and stability in aqueous KOH solution. Finally, CO_2 solubility and mass transfer coefficient were determined and correlated with membranes' performance in the direct air capture device. In general, it was found that the presence of the additive greatly improved the characteristics of the membranes in terms of CO_2 capture efficiency and robustness, outperforming the results obtained previously. The best results for were obtained with 5% additive content reaching 0.18 [mol/m^{2}s].

1. Introduction

Fossil fuels are the most important source of energy with almost no alternatives. Power plants burn fossil fuels to produce electricity and energy. Therefore, post-combustion gases released are considered the main factor for emission increase. The energy industries based on fossil fuels, such as petroleum, coal, natural carbon dioxide gas and metal processing, are not only the centerpiece of economic development but also the main body of CO_2 emissions, together with the transport section with special emphasis on thermal engines. Atmospheric CO_2 concentration has become a subject of worldwide concern because it seriously contributed to global warming and climate change, which resulted in serious environmental problems [1,2]. The report of the International Panel on Climate Change (IPCC) showed that modelled pathways which aim at limiting global warming to 1.5 °C, involve fast and, in most cases, immediate greenhouse gas emissions reductions in all sectors this decade and that global net zero CO_2 emissions must be reached in the early 2050s. Otherwise, human beings could face the most damaging effects emerging from climate change [3,4]. On the other hand, in 2050 global energetic demand will rise about 15% versus 2021, with electricity demand projected to grow between 62% and 185% in the same period, as recently pointed out by The International Energy Agency (IEA) [4]. Even with the rapid development of renewable energies, most of electricity would still come from fossil fuel for the next few decades, which makes the CO_2 emission reduction a major challenge. Hence, it is necessary to explore low energy-consumption, cost-effective, available and efficient technologies for the capture and separation of CO_2 produced by the industrial sources.

Emissions can be reduced by decreasing the energy consumption or using natural renewable energy sources; however, the carbon dioxide present in the atmosphere can be decreased by its capture. Several methods have been identified for the removal and capture of CO_2 based on physical and chemical processes: absorption, adsorption, conversion, cryogenic separation, and membrane techniques [5–7]. However, membrane technology holds great promises for CO_2 capture by gas-liquid absorption. It has several attractive advantages compared to

* Corresponding author.
E-mail address: marta.giamberini@urv.cat (M. Giamberini).

https://doi.org/10.1016/j.jcou.2023.102629
Received 5 September 2023; Received in revised form 10 October 2023; Accepted 14 November 2023
Available online 21 November 2023

other CO_2 capture methods: high energy efficiency, cost effective method, compact and portable systems that are simply operated [8]. Recently, new hybrid processes have been studied, they take advantage from advanced membrane technologies and CO_2 absorption methods in a single device. In these devices, the membrane plays the role of a physical barrier that separates the two phases; this system is called a contactor [6,7]. In membrane contactors, CO_2 absorption occurs when a gas stream enters the system through the membrane pores and gets in contact with the aqueous absorbing solution that flows in the opposite side of the membrane [8,9]. Therefore, the surface area for phase contact increases, which facilitates the mass exchange process [10]. On the other hand, membrane pores should be filled with gas to prevent any membrane wetting. Consequently, membrane mass transfer resistance decreases while CO_2 flux increases [9,11,12].

Direct air capture is currently considered as an emerging technology for carbon dioxide removal, which includes geological storage of biotic carbon and the acceleration of geochemical weathering [13]. The capture of carbon dioxide from the atmosphere was proposed as a possible cost-competitive climate mitigation technology [14]. Regarding this aspect, nature represents a great inspiration, since photosynthesis occurring in leaves represents an efficient and optimized process for air capture. In more details, photosynthesis takes place through stomata, which are the organs used to control the gas exchange in leaves. They are in charge of controlling the exchange of gases - especially water vapor and CO_2 - between the interior of the leaf and the atmosphere [15]. Nogalska et al. reported a biomimetic contactor, a system that simulates the stomata, based on a polysulfone membrane and a potassium hydroxide solution used as an absorbent, which is in direct contact with the bottom side on the membrane[16]. For this system, CO_2 absorption was greatly improved with respect to the value of natural stomata (20 μmol/(m^2 s)) [17].

The common materials for CO_2 removal membranes are organic polymers. Polysulfone is widely employed as an asymmetric porous membrane in different gas separation and absorption processes [18,19], due to its relatively high CO_2 permeability. Furthermore, polysulfone membranes have excellent mechanical strength, high thermal and chemical stability but also good hydrophobicity and low mass transfer resistance for CO_2 [20]. All these properties above make this polymer a good choice for membrane gas absorption processes [21].

Amines are currently the most efficient and cost-effective materials for CO_2 capture [22,23]. It is often mentioned that primary amines are more reactive towards CO_2. However, in order to fully investigate the effects of amines on CO_2, the electronic and steric effects of all substituents attached to the nitrogen atoms should be considered. Furthermore, the basicity of amines is the most critical factor that affects CO_2 capture performance due to the acid/base reaction between CO_2 and amines. The reaction between CO_2 and a primary or secondary amine that are sterically unhindered forms a stable carbamate. Only half mole of CO_2 is absorbed per mole of amine group (Scheme 1.a). However, it was shown that the formation of some hydrogen carbonate could increase this sorption ratio (Scheme 1.b). Since the carbamate is fairly stable, the absorbent regeneration is difficult due to the high amount of heat energy needed to break the bonds [24]. In contrast, tertiary and hindered amines form an unstable carbamate and, due to a hydrolysis reaction, lead to the formation of hydrogen carbonate ions, which results in a loading capacity of one mole CO_2 per mole of amine group (Scheme 1.c) [25]. Aqueous amine solutions, such as mono-(MEA) and diethanolamine (DEA), have been used to capture CO_2 and generate food-grade carbon dioxide in the natural gas industry since decades [26].

$$\tfrac{1}{2}\,CO_2 + R_2NH \rightarrow \tfrac{1}{2}\,R_2NCOO^- + \tfrac{1}{2}\,R_2NH_2^+ \quad (a)$$

$$CO_2 + R_2NH + H_2O \rightarrow HCO_3^- + R_2NH_2^+ \quad (b)$$

$$R_2NCOO^- + H_2O \rightarrow HCO_3^- + R_2NH \quad (c)$$

Scheme 1. Equations of: (a) Carbamate formation; (b) Hydrogen carbonate formation; (c) Carbamate reversion to hydrogen carbonate.

Aqueous amine absorption is practical to capture CO_2 from gas streams with a low partial pressure of CO_2. However, amine solutions are limited to be used with low concentrations for different processes in CO_2 recovery plants, due to equipment corrosion and amine solvent degradation caused by oxygen present in aqueous solution [27]; however, the biggest issue is the high heat capacity of the amine solution that occurs in the aqueous phase for CO_2 capture, which causes a high energy consumption. Moreover, technical scalability limits its application to CO_2 capture from flue gas emissions of electricity power plants that burn coal or natural gas. For that reason, CO_2 capture by using solid adsorbents, such as polyamines, is considered as a promising alternative to avoid all problems related to aqueous amine absorbents. Polyamines are being intensively investigated by loading and blending them with other support materials, such as membranes. Therefore, polyethyleneimine (PEI) is the most investigated because it is relatively cheap, easily synthesized and more thermostable compared with other amine-based adsorbents or amine oligomers [28]. Since PEI was introduced for CO_2 capture in space shuttle applications by Satyapal et al.[29], many researchers have studied PEI as an adsorbent for CO_2 capture by loading it on many support materials.

In a previous paper, we tried to improve the performance of polysulfone (PSF) membrane contactor used for CO_2 capture from ambient air as reported by Nogalska et al. [16], by blending polysulfone with a commercial hyperbranched polyethylene imine, namely Lupasol G20, chemically modified with benzoyl chloride at partial extent (aromatic groups/nitrogen atoms content around 19%), to give mG20 additive [30]. The partial chemical modification of Lupasol G20 was carried out in order to decrease its water-solubility; in this way, the blended PSF membranes could be prepared by phase inversion precipitation in a water coagulation bath and a porous asymmetric membrane was prepared. We found that the addition of the polymer resulted a 4-fold increase of CO_2 flux with respect to neat PSF membrane; on the other hand, increased absorbent (KOH solution) uptake and eventual K_2CO_3 formation, from the reaction of CO_2 with KOH, resulted in pore clogging and was evidenced when the additive amount was higher than 5 wt%. This determined worse performances in terms of CO_2 assimilation in those cases. On the other hand, it must be also pointed out that the chemical modification reaction took place on primary and secondary amines of the Lupasol G20 structure, consequently forming hydrochloric acid (HCl) as a byproduct (Scheme 2) that could be trapped on the membrane matrix and affect both CO_2 capture and membrane stability.

For this reason, in the present paper we investigated a different approach for Lupasol G20 chemical modification to increase both, its hydrophobicity and stability of the final blended membrane. Here, Lupasol G20 was partially modified by a solvent-free, eco-friendly method [31], by phenyl isocyanate; in this way, we obtained UG20 additive, with decreased water-solubility. Consequently, this converted the sterically unhindered nitrogen atoms into sterically hindered ones by forming urea groups; moreover, these groups are more basic compared to the amide formed in the previous modification by benzoyl chloride. Additionally, the stability of the membrane is expected to increase as well, since the reaction performed produces no side product that could be trapped in the polymer. PSF-based membranes with different amounts of the modified Lupasol G20 were studied (specifically 2, 5 and 10 wt% with respect to PSF) and compared to pristine PSF membrane.

2. Materials and methods

2.1. Materials

Polysulfone (PSF, MW 35000 Da) in transparent pellet form, phenyl isocyanate (98%) and 1-methyl-2-pyrrolidone (NMP, ACS) were purchased from Sigma-Aldrich (Sigma Aldrich Química, Madrid, Spain) and

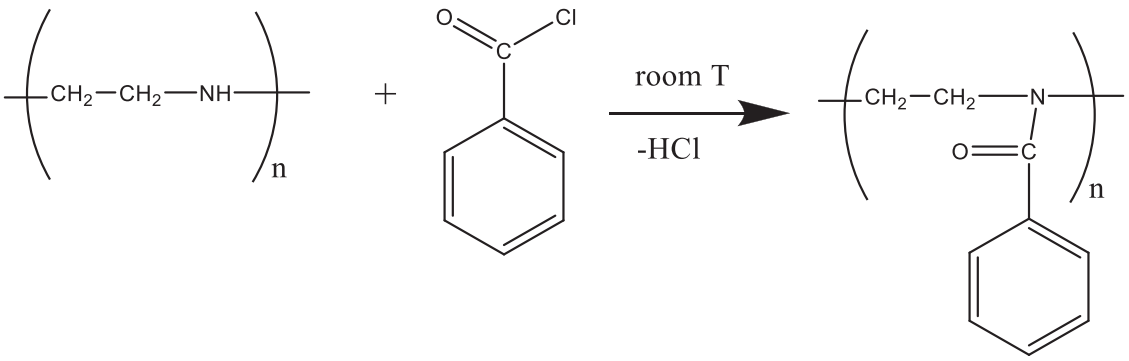

Scheme 2. Reaction of PEI (Lupasol G20) with benzoyl chloride.

used as received. Polyethyleneimine (PEI) (Lupasol G20, 1300 g/mol) was kindly provided by BASF (Tarragona, Spain) and used as received. Its structure is reported in Fig. 1.

Low conductance (Milli-Q®) water was used in a coagulation bath for membrane preparation. Extra pure potassium hydroxide in pellets (Scharlab, Barcelona, Spain) was dissolved in deionized water to prepare solutions for membrane swelling and to be used as absorbent in DAC system. Potassium hydrogen phthalate (>99.95% purity) was purchased from Aldrich and used as a standard in ^{1}H NMR analysis.

2.2. Additive preparation

Lupasol G20 was partially chemically modified to decrease its water solubility. As seen for primary amines in Scheme 3, we used a solvent-free, eco-friendly method which did not require any organic solvent. The modification of PEI was performed with 25% of stoichiometric amount of phenyl isocyanate with respect to the cationic charge density of Lupasol G20 (17 meq/g) by adding 5.1 g drop-wise directly to 10 g of Lupasol G20 magnetically stirred for two hours at room temperature. The reaction was then left overnight. The resultant product was carefully washed three times by distilled water under stirring, to remove the water soluble residue, which resulted in UG20, an oily product that was left to dry for 24 h. The modified Lupasol G20 was finally analyzed by ^{1}H NMR, as can be seen in Fig. S1 in Supplementary Information. The final modification degree was found to be around 17%.

2.3. Membrane preparation

All polysulfone-based membranes were prepared by phase inversion process, namely immersion-precipitation, in ambient conditions. N-Methylpyrrolidone (NMP) was used to dissolve 20 g of PSF/UG20 blending so that the total polymer concentration would be fixed at 20 wt % with respect to total polymeric solution weight. Polymer blends were stirred for 48 h, then left for bubble removal. Subsequently, polymer solutions were cast on a glass using a 250 μm casting knife, and instantly put into a Milli-Q water coagulation bath. The membranes precipitated as a result of solvent and non-solvent exchange, NMP and water, respectively. The top surface of the prepared membranes is the one in contact with the coagulation bath, while the bottom is the one in contact with the glass in the first instances of the precipitation process. Resulting flat sheet membranes were removed from bath, washed for 24 h in Milli-Q water and left to dry on air after the washing process. In this article M0 will be referring for neat PSF membrane, whereas M2, M5 and M10 will be referring for membranes containing 2, 5 and 10 wt% of UG20 relative to PSF (weight ratio basis), respectively.

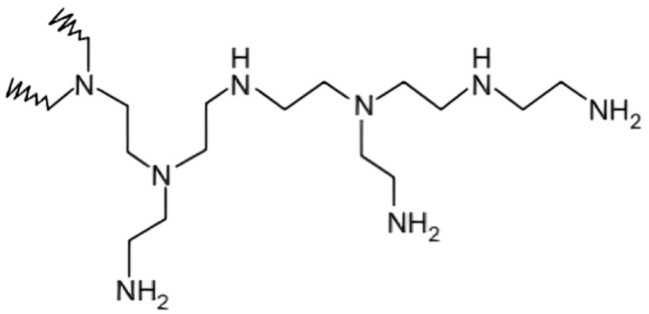

Fig. 1. Chemical structure of Lupasol.

2.4. Characterizations

^{1}H NMR spectra of UG20 in deuterated methanol (CD_3OD) were recorded at 400 MHz on a Varian Gemini 400 spectrometer. A pulse delay time of 5 s was used. The solvent peak was taken as the reference, and the chemical shifts were given in parts per million from TMS (Tetramethylsilane). Additionally the polysulfone membranes were characterized by the same technique. Membrane samples (10–20 mg) were dissolved in dimethylformamide-d6 (dmf-d6) together with a known amount of potassium hydrogenphthalate (5–10 mg) as the internal standard for the quantification of residual N-methylpyrrolidone (NMP). Dimethyl sulfoxide-d6 (dmso-d6), in a sealed co-axial capillary tube, was used as the deuterium reference external standard. The amounts of NMP were determined from the ratio of the NMP and potassium hydrogenphthalate signals (δ: 1.93 and 7.49 ppm, respectively) after baseline correction.

The membrane surface morphology and roughness were determined by Atomic Force Microscopy (AFM) – Molecular imaging model Pico SPM II (Pico+) (scan size: 2 μm × 2 μm, WsxM software).

Field Emission Scanning Electron Microscopy (FESEM) by means of Scios2 microscope (Thermo Fisher Scientific, Waltham, USA) was used to analyze the internal morphology of membranes. Electrons were accelerated at 5.00 kV, the working distance was comprised between 3 and 7 mm and ETD or T2- high resolution secondary electrons detectors were used. Membranes were previously criofractured in liquid nitrogen in order to observe their cross sections. Elemental analysis was performed by means of Thermo Fisher Scientific EDX analyzer equipped with Pathfinder software on the aged samples.

The glass transition temperatures (Tg) of M0-M10 membranes were determined by Differential Scanning Calorimetry (DSC) by means of Mettler DSC-821e device, calibrated using an In standard (heat flow calibration) and an In-Pb-Zn standard (temperature calibration). Samples (≈ 5 mg) were tested in aluminium pans with a pierced lid in N_2 (50 mL/min) in dynamic mode at a heating rate of 10°C/min from 0°C to 200°C; Tg was determined as the inflection point in the heat flow signal step.

Dielectric thermal analysis (DETA) was used to provide information on the molecular structure of the membranes and molecular mobility. Impedance measurements were conducted using a Novocontrol Broadband Dielectric Impedance Spectrometer (BDIS), connected to a

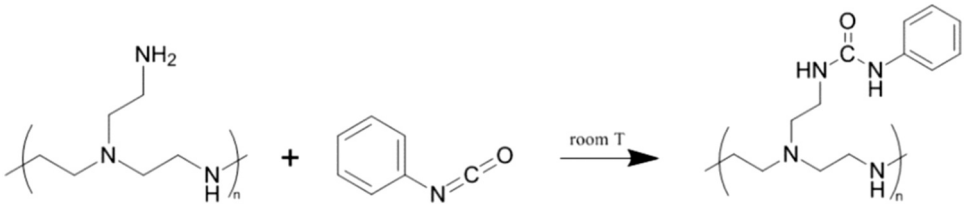

Scheme 3. Reaction between Lupasol G20 and phenyl isocyanate.

Novocontrol Alfa-A Frequency Response Analyzer. The measurements were obtained under isothermal conditions in the frequency range of 10^{-2} to 10^{7} Hz, increasing the temperature in steps of 10 °C between − 150° and 250°C.

Raman spectra of the blended membranes were recorded by means of inVia™ confocal Raman microscope Renishaw (Agilent) for UG20 additive, neat PSf and M10 membrane under 785 nm laser excitation (10% Power, diffraction grating: 1200 l/mm, exposure time: 50 s, objective x50). The analysis was performed at different depth layers for each sample, i.e. top surface, center (50 and 100 μm deep) and bottom surface.

Fourier transform infrared spectroscopy (FTIR) analysis of as prepared or aged membranes (M0-M10) was performed using VERTEX 70 (Bruker) to study the chemical composition as well as the possible hydrolysis of urea groups in our membranes. Spectra of aged membranes were acquired after soaking in aqueous KOH (0.64 M) with software OPUS 7.0 (Bruker Optics Inc.). Subsequently, we studied the effect of UG20 content increase on the chemical composition of the membrane in both, treated and untreated cases.

The overall membrane porosity (ε), defined as the volume of the pores divided by the total volume of the membrane, was determined by using a method based on the density measurements according to the following equation:

$$\varepsilon \quad (\%) = (1 - \rho m/\rho p) \times 100 \tag{1}$$

where ρ_p corresponds to the polymeric material density, which is a weighted average of polysulfone (1.24 g/cm^3) and UG20 (1.08 g/cm^3) density, and ρ_m to the membrane density. The membrane density is calculated by determining the relationship between mass and volume (thickness multiplied by area) of 1 cm^2 of membrane.

Specific surface areas and pore volumes were measured by N_2 physisorption at − 196 °C by QUADRASORB SI surface analyzer, Quantchrome Instruments, equipped with FloVac Degasser, FloVacTM. Samples were previously degassed in situ at 80 °C overnight under vacuum. Surface areas were calculated using the Brunauer-Emmet-Teller (BET) methods over a P/P^0 range where a linear relationship was maintained. Pore size distribution was predicted from the desorption wing of the isotherm by applying the Barrett-Joyner-Halenda (BJH) method. The membranes cross-sections obtained by cryofracture were examined by ESEM before and after degassing, in order to verify that degassification did not alter their inner structure.

Mechanical properties of all membrane samples were analyzed using stress-strain measurement. Tensile measurements were performed via an Instron-5564 (Instron, MA, USA) instrument with a sample dimension of 10 × 50 mm, and a gauge length of 28 mm, at ambient atmosphere (25 °C, ~40% relative humidity), and a deformation rate of 5 mm/min.

Water and KOH uptake tests were performed on previously dried membranes (size: 1.5 ×3 cm^2). The membranes were dried at 60 °C for 72 h, weighed, soaked in Milli-Q water or KOH 0.64 M solution under stirring for 24 h at room temperature, and reweighed. The water or KOH uptake (*Upt*) was calculated as:

$$Upt(\%) = \frac{W_{wet} - W_{dry}}{W_{dry}} \times 100 \tag{2}$$

Where W_{wet} is the weight after soaking and W_{dry} the initial weight after drying.

Water contact angle of the membranes was determined by Dataphysics PCA 15EC. A 3 μL droplet of Milli-Q water was placed on the surface of the membrane and the contact angle was calculated from a digital image by software composition analysis (SCA) (DataPhysics, Fildertstadt, Germany) included in the apparatus. Contact angle values were taken as the average of three measurements.

2.5. CO_2 permeability and solubility measurements

A self-made, stainless-steel module, dead-end apparatus with an embedded membrane was used to measure the carbon dioxide permeance (Fig. 2). Pure CO_2 or N_2 was injected into the module containing the membranes with an effective area of 16 cm^2. Gas permeation tests were conducted at 1, 2, and 3 bar, respectively, by measuring pressure increase in the permeate compartment using a precision gas pressure sensor (stork solutions model: UPS-HSR-B02P5G). Mass transfer coefficient k (mol/(s m^2 bar)) was calculated following the Eq. (3):

$$k = n/(A \cdot \Delta P) \tag{3}$$

Here, n stands for molar flow (mol/s), A is membrane area (m^2), and ΔP is the pressure gradient (bar).

The solubility of CO_2 was investigated using the pressure decay method (Fig. 2), whereby membrane samples (≈ 150 mg) were placed in the bottom of the module and carbon dioxide was injected into the system to reach 2 bar. When the pressure reached 2 bar, the valve was closed, and the pressure decrease until equilibration was measured by a digital pressure sensor. The solubility of materials was calculated following the Eq. (4):

$$n_{CO_2} = \frac{(p_i - p_f)V}{RT} \tag{4}$$

where n_{CO2} is the adsorbed moles of CO_2, p_i and p_f are the initial and final pressures (Pa), respectively, V is the gas volume(m^3), R is gas constant (8.314 J/(K·mol)), and T (K) is temperature. The solubility coefficient, S_{CO2} (m^3 (STP)/(m^3·atm)), which is used to indicate the solubility of gases, is calculated according to Eq. (5):

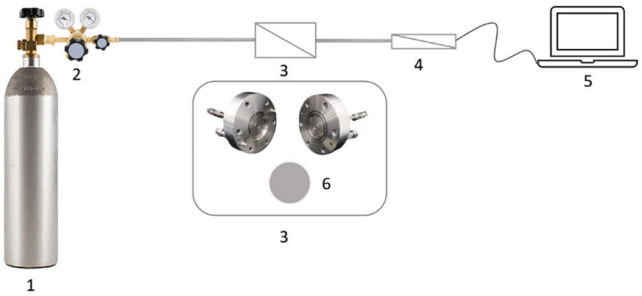

Fig. 2. Setup for solubility and permeability measurements: (1) N_2 or CO_2 gas tank, (2) Valve, (3) Steel module containing membrane, (4) Digital gas pressure sensor, (5) Computer, (6) Membrane.

$$S_{CO2} = \frac{V_{co_{2m}}\ (STP)}{V_m P_{estabilished}} \quad (5)$$

where V_{CO2m} (STP)(m^3) is the volume of CO_2 relating to n_{CO2} at STP conditions (1.013×10^5 Pa, 273.15 K, recalculated from eq. 4), V_m is the analyzed material volume (m^3, taking into account the porosity), and $P_{established}$ (atm) is the pressure measured at equilibrium conditions.

2.6. Direct air capture measurements

The direct air capture CO_2 absorption test was carried out in a gas-liquid membrane contactor, with home-made module as described in Fig. 3 and [16]. The prepared membranes were placed in a module, where the top surface was exposed to ambient air (no pressure or flow applied) by holes in the cover of the module and the bottom surface (9 cm^2 contact area) of the flat sheet membrane is in contact with 10 mL of the 0.64 M KOH solution as a liquid absorbent. The total of 100 mL of the absorbent was circulating between the reservoir and the module thanks to the pump in a different range of flow rate from 40 to 340 mL/min at room conditions (25 °C and 1.013×10^5 Pa). The experiments were conducted for 1 h with continuous stirring, and each one was repeated three times with a new membrane to verify the reproducibility. After 1 h, samples were collected, and the absorbed CO_2 amount was determined by means of a carbon dioxide ion-selective electrode (Hanna HI4105 connected with Orion Dual Star pH/ISE Benchtop meter), according to the procedure reported next:

Diluted samples (1 mL) were mixed with 43 Milli-Q water, 1 mL standard (0.1 $NaHCO_3$) and CO_2 buffer (5 mL, Orion Application Solution 950210) to adjust the pH to the electrode working pH at 4.8–5.2. The concentration of total carbonic species (CO_3^{2-}, HCO_3^- and CO_2) was determined after calibration with $NaHCO_3$ standard (0.1 M), and buffer. The stable value of CO_2 absorption flux (mol/m^2·s), J_{CO2}, according to Yeon and Lin [32,33] was calculated by the following Eq. (6):

$$J_{CO2} = \frac{Q_i . M_{CO2}}{A} \times 1000 \quad (6)$$

where Q_i stays for the absorbent flow rate (m^3/s), M_{CO2} is the CO_2 concentration in the absorbent (mol/L) obtained from the ISE measurements, and A is the area of the flat sheet membrane (m^2).

3. Results

3.1. Additive synthesis, blended membrane preparation and morphological characterization

^{1}H NMR of the modified Lupasol (UG20) in deuterated methanol (Fig.S1) shows two groups of broad, partially overlapped signals, in the regions 6.5–7.8 ppm (aromatic protons) and 2.2–3.8 ppm (ethylenic protons adjacent to nitrogen atoms), proving that the chemical modification with phenyl isocyanate was successful [34]. According to Lupasol G20 structure (Fig. 1.), the ratio N:C is 1:2: therefore, approximately each ethylene group corresponds to one nitrogen atom. So, we could roughly estimate the ratio of bonded aromatic groups (i.e. reacted phenyl isocyanate) vs. ethylene groups, i.e. aromatic groups/nitrogen atoms content, based on the integration of the aforementioned signals. This is directly related to the achieved modification degree, which resulted around 17%. Taking into account that the phenyl isocyanate amount used in the reaction corresponded to 25% of the cationic charge density of Lupasol G20, one can conclude that the chemical modification of the hyperbranched PEI occurred at good extent. Actually, this degree of modification reduced Lupasol G20 solubility in water sufficiently so to allow blended membrane preparation by phase inversion precipitation in water as desired. In our previous paper [30], Lupasol G20 turned out to be modified by benzoyl chloride at around 19%, yelding mG20 additive: therefore, UG20 and mG20 can be considered comparable in terms of grafting amounts.

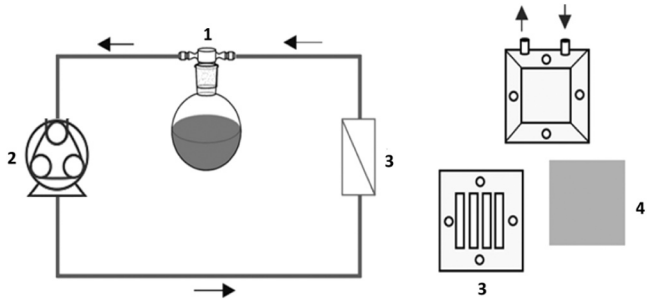

Fig. 3. Direct air capture system for CO_2 absorption: (1) KOH solution tank, (2) Pump, (3) Module containing membrane, (4) Membrane.

Unfortunately, the exact amount of additive finally contained in the obtained membranes could not be determined by ^{1}H NMR, due to the presence of very broad and partially overlapped signals in both polymeric components, which prevented an accurate integration. Therefore, the additive amount mentioned throughout the paper corresponded to the theoretical amount calculated based on the initial polymeric solution, assuming that none of the additive was washed out in the precipitation process. The importance of carefully washing the membranes after their precipitation should be also underlined. When membranes were washed with water just for 30 min, 7–8 wt% of residual NMP was detected by ^{1}H NMR. Fig.S2 shows the ^{1}H NMR spectrum of M0 membrane washed for 30 min as a matter of example. In this spectrum, the peaks relative to residual NMP can be clearly distinguished and allowed the quantification of residual NMP after washing, by means of potassium hydrogen phthalate as internal standard. NMP acts as a plasticizer, as it will be shown in Section 3.3. However, careful ^{1}H NMR analyses of washed samples assured that 24 h were a sufficient to completely remove NMP from the prepared membranes.

The composition and morphological characteristics of the membranes under study are shown in Table 1.

Environmental scanning electron microscope (ESEM) was used to characterize the membrane morphology, in which membrane thicknesses were obtained by ESEM micrographs analysis with ImageJ software. Thickness values presented in Table 1 correspond to the average of three measurements.

Thickness values range around 140–150 μm. Fig. 4a-d show the cross-sectional images of M0, M2, M5 and M10 membranes. ESEM could not clearly evidence internal structure changes when UG20 additive content increases, i.e. a similar morphology can be noticed, which reveals the same finger-like structure for pores with a spongy and denser layer on the bottom. The amount of macrovoids looks the same as we increased UG20 content. Macrovoids can be explained as a consequence of the instantaneous demixing that occurs when the casting solution and the coagulant get in contact and they are associated with instantaneous precipitation and lower viscosity of the polymeric solution [35]. This leads to a fast penetration of water, as a non-solvent, into the polymeric solution. This phenomenon determines highly asymmetric structures, with fingerlike macrovoids; on the other hand, slower coagulant penetration induces slower precipitation and finally forms sponge-like, more symmetric structures [36]. Furthermore, it has been also shown that the evolution from a spongy-like to a macrovoid morphology also depends

Table 1
Composition and morphological characteristics of studied membranes.

Membrane	UG20/PSF (wt%)	Thickness (μm)	Specific Surface Area (m^2/g)
M0	0	142 ± 1	27.4
M2	2	146 ± 5	28.2
M5	5	137 ± 4	12.5
M10	10	150 ± 4	6.3

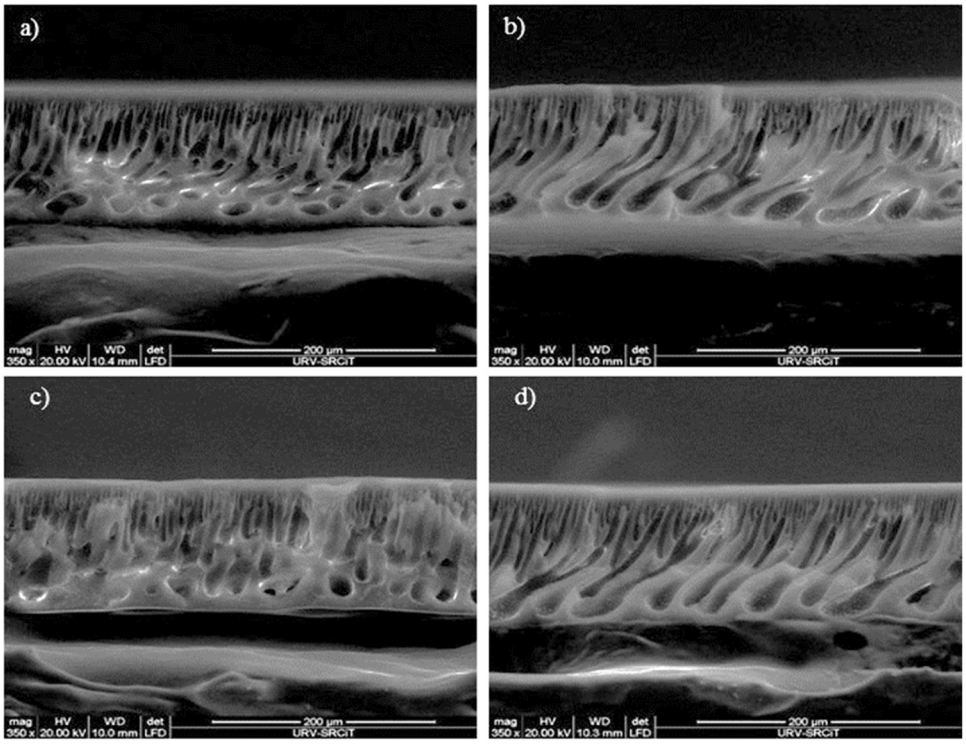

Fig. 4. Environmental scanning electron microscope (ESEM) cross-sectional images of studied membranes: (a) M0; (b) M2; (c) M5; (d) M10.

on the membrane thickness; a full development of a fingerlike structure can be observed when thickness is higher than a critical value, which varies according to the whole system composition [37]. In our case, membrane thicknesses all lie within 140 and 150 µm approximately (Table 1), which should lead to fingerlike morphologies. On the other hand, since UG20 is a hydrophilic polymer, it should contribute to slower the precipitation of PSF-based membranes, and therefore should lead to a less porous structure. Also, one should remember that the solution viscosity also plays a role in the phase inversion process, since it may alter the precipitation rate and, consequently, membrane morphology. Therefore, the higher the additive content, the higher the difference in the solution viscosity, which could slow down the miscibility of polymeric solution and water. In our previous paper [30], when the used additive was Lupasol G20 modified with benzoyl chloride at similar extent (mG20), we could find a remarkable effect of the additive content on membrane morphology just in the case of 20 wt% additive amount; nevertheless, some evidence of a growing dense layer were already shown by the sample containing 10 wt% additive. However, for that system, in the absence of a more exhaustive analysis of porosity, a change in morphology with additive increase could not be ruled out.

The overall porosity of M0-M10 membranes, as calculated by density measurements, did not show any significant difference within the experimental error, being approximately 72% in all cases. Therefore, in order to get further insight into membrane porosity of M0-M10 systems, nitrogen adsorption and desorption isotherms were determined and analyzed. Table 1 shows acquired cumulative BET surface area, while Fig. 5 depicts cumulative pore volume for M0-M10 membranes.

The adsorption isotherms of these samples were mainly of type II corresponding to non-porous materials, with some hysteresis loop, which also envisages some macro- or mesoporosity [38]. Therefore, a wide range of size and shapes can be expected. As a matter of example, Fig.S3 shows the adsorption isotherms of M0 and M10. From physisorption data, a wide range of pore size could be evidenced, ranging between 15 and 4000 Å approximately. From Table 1 and Fig. 5, it can be noticed that the addition of 2% UG20 (M2 sample), does not significantly alter neither the total pore volume and nor the surface area with

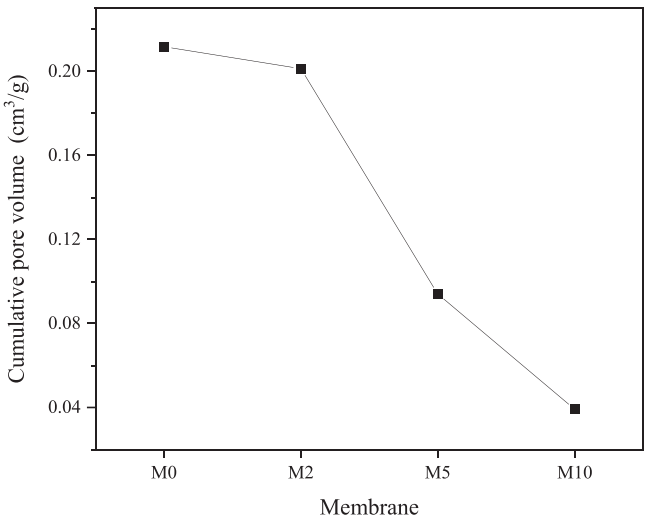

Fig. 5. Cumulative pore volume of M0-M10 membranes.

respect to M0. On the other hand, as a general trend, the presence of increasing amounts of additive (M5 and M10 samples) determines a general decrease of porosity and porous surface area. As for the pore volume distribution in the final membranes, Fig.S4 shows the full range for the whole set of membranes, while Fig. 6 reports the zoom corresponding to pore radii between 0 and 150 Å, i.e. covering micro- and mesoporosity ranges, for M0, M5 and M10 samples.

In general, one can see that increasing addition of UG20 (M5 and M10 samples), displaces the distribution of pore size towards lower values (Fig. 6 and Fig.S4). This can be attributed to a progressive delayed demixing which occurs when the concentration of UG20 increases, probably as a consequence of different affinity for the coagulant of the blended polymeric solution.

PSF-based membranes were characterized in terms of surface

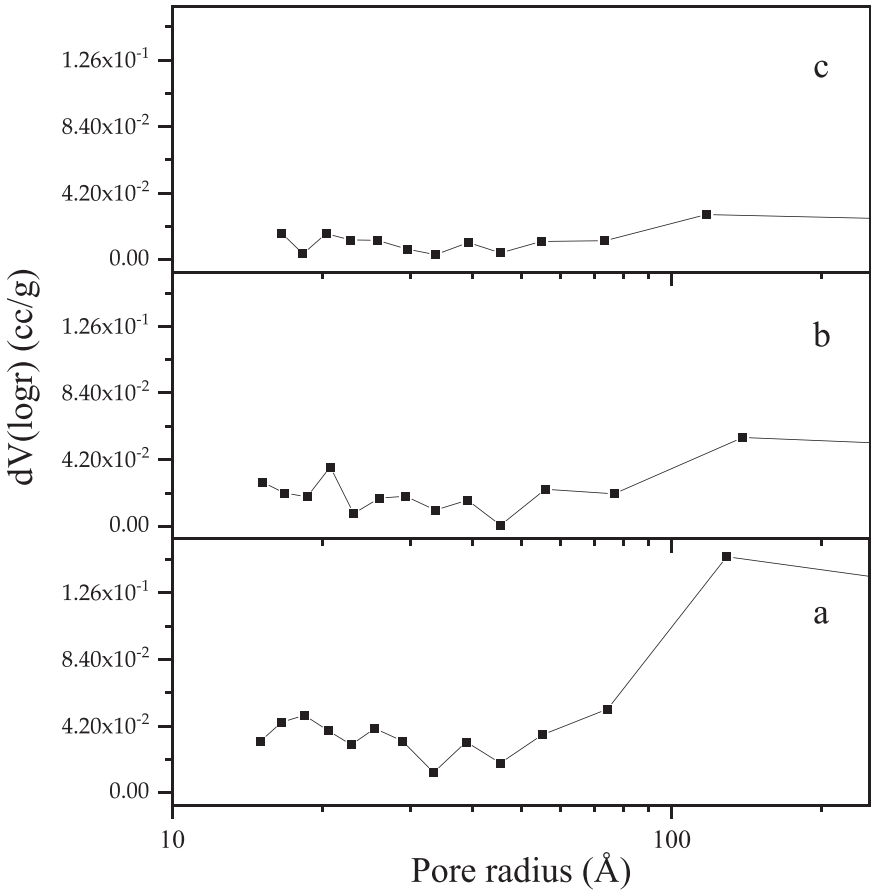

Fig. 6. Pore volume distribution zoomed between 0 and 250 Å of: (a) M0; (b) M5; (c) M10.

roughness and stability. Both water contact angle and swelling tests were performed in order to investigate the effect of UG20 content on the wettability of blended membranes compared to neat PSF. Root-mean-square (RMS) roughness was investigated on the bottom side of membranes, since in membrane contactors, the bottom side of membranes is in direct contact with the absorbent aqueous solution and the higher are the roughness parameters the higher is the contacting area. The RMS roughness parameters of bottom side of M0-M10 membranes were determined from three-dimensional topographic AFM images seen in Fig.S5a-d. Table 2 reports the bottom side RMS roughness, water contact angle values and water and KOH (0.64 M solution) uptake of the membranes.

Membrane surface wettability was investigated by means of water contact angle measurements. When UG20 is present in the blended membranes (samples M2-M10), within the experimental error, the contact angle values slightly decrease on the top of the membrane with respect to neat PSF (sample M0), while they keep practically constant on the bottom side of the membrane. Initially, this could suggest that UG20 is more prominent on the top side of the membrane due to more hydrophilic character of the additive with respect to PSF. As for surface morphology, we determined the RMS roughness from AFM topographic images, shown in Fig.S5, of the membranes' bottom side, which is directly in contact with the alkaline solution in the CO_2 capture device. A slight increase in RMS roughness was observed for the membranes containing higher amounts of UG20, i.e. M5 and M10; nevertheless, it does not seem to affect significantly the CA values of the corresponding samples.

As shown in Table 2, when UG20 content increases, both water uptake (WU) and KOH uptake of blended membranes tend to increase as well, as expected due to the more hydrophilic character of UG20 additive. Higher WU and KOH uptake can be intrinsically related to a lower absorption flux. Indeed, pore wetting can negatively affect gas diffusivity and provoke pore clogging. This effect is visible when working in membrane contacting system with KOH solution as absorbent. Nevertheless, WU and KOH uptake of M2-M10 samples are much lower compared to PSF membrane additivated with mG20 additive previously reported [30], which suggests better performances. Actually, WU of PSF/mG20 ranged between 6% and 274%, while KOH uptake after 24 h resulted as high as 22% even in the case of 2% additivated membrane. For higher mG20 amounts, it could not be determined: indeed, after soaking 24 h in 0.64 M KOH, PSF/mG20 samples exhibited weight loss, due to the basic hydrolysis of the ester bonds in the additive.

Table 2
Root-mean-square (RMS) roughness of bottom side, water contact angle (CA), water uptake (WU) and KOH (0.64 M solution) uptake of the studied membranes.

Membrane	Bottom RMS roughness (nm)	Top CA (°)	Bottom CA (°)	WU (%)	KOH uptake (%)
M0	10.8	76±3	69±3	0.6 ± 0.2	1.5 ± 0.1
M2	10.6	67±2	72±1	2.3 ± 0.3	2.3 ± 0.2
M5	11.4	68±3	67±2	7.4 ± 0.2	4.4 ± 0.6
M10	15.6	64±2	67±2	10.4 ± 0.6	9.4 ± 0.4

3.2. Additive distribution and membranes' chemical stability

In order to get insight into the distribution of UG20 additive in PSF membranes, first we analyzed Raman spectra, obtained by a 785 nm excitation laser, across the section between 200 and 2000 cm^{-1}. Fig. S6 (Supplementary material) shows the Raman spectra registered on top surface of M10 membrane, pure UG20 additive and neat PSF membrane (M0). Different bands can be attributed to the additive, without overlapping those of neat PSF membrane. The 1030 cm^{-1} band in Fig. S6(a) can be attributed to the C-N stretch for secondary and tertiary aliphatic amines that is suggested to be a shoulder in the M10 Raman spectrum [39,40]. On the other hand, the shoulder at 1651 cm^{-1} is typical for urea compounds, and it is related to C═O stretching in urea (Amide-I region). Unfortunately, this shoulder found in UG20 spectrum (as seen in Fig.S6 (a)) is not visible even in M10 spectrum (Fig.S6(b)), that is the membrane with the highest additive content. This is probably due to the low content of UG20 in the membrane compared to the polysulfone and the detection limits. Similarly, no differences could be detected when M10 membrane was studied at different depth layers, namely top surface, center (50 and 100 μm) and bottom surface. Fig. S7 in Supplementary Information shows the Raman spectra of different layers (Top, center and bottom) in M10 membrane; all the peaks can be overlapped. Therefore, we could not determine the exact distribution of UG20 throughout the blended membranes.

Since the additivated membranes were prepared to be used in contact with 0.64 M KOH solution in the direct air capture device, it is convenient to study their stability to the alkaline environment. PSF is well known for its excellent chemical stability in alkaline environment [41]: therefore, the chemical stability and good performance of M2-M10 membranes are essentially determined by the stability of the contained UG20 additive.

Fig. 7 shows the FTIR spectra between 500 and 200 cm^{-1} of M0-M10 membranes. The broad band highlighted by an arrow around 1660 cm^{-1} in Fig. 7d can be attributed to the C═O stretching in urea. This band is more visible and prominent as UG20 additive content increases, i.e. in M10 which is the membrane with the highest UG20 content. Therefore, the study of stability was focused on M10 sample, where variations of band intensity could be more clearly evidenced.

Fig. 8 depicts the FTIR spectra between 1000 and 2000 cm^{-1} of (a) fresh M10, (b) M10 after soaking 24 h in 0.64 M KOH and (c) UG20 additive.

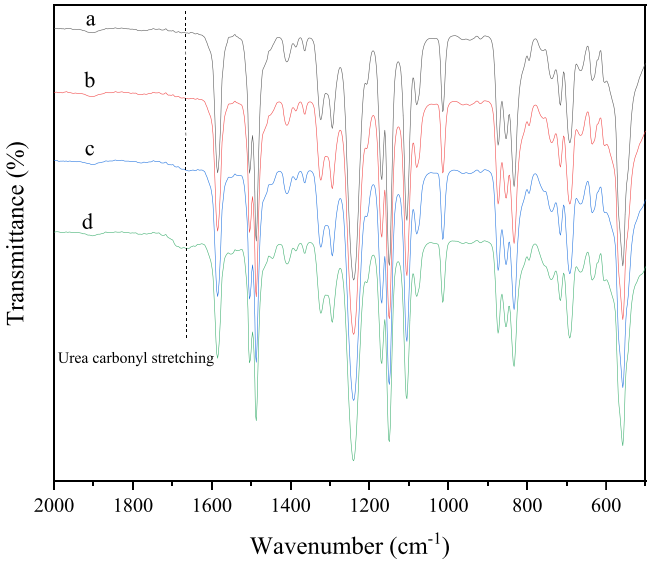

Fig. 7. Infrared spectra between 500 and 2000 cm^{-1} of: (**a**) M0; (**b**) M2; (**c**) M5; (**d**) M10. The band relative to C═O stretching of urea around 1660 cm^{-1} is highlighted.

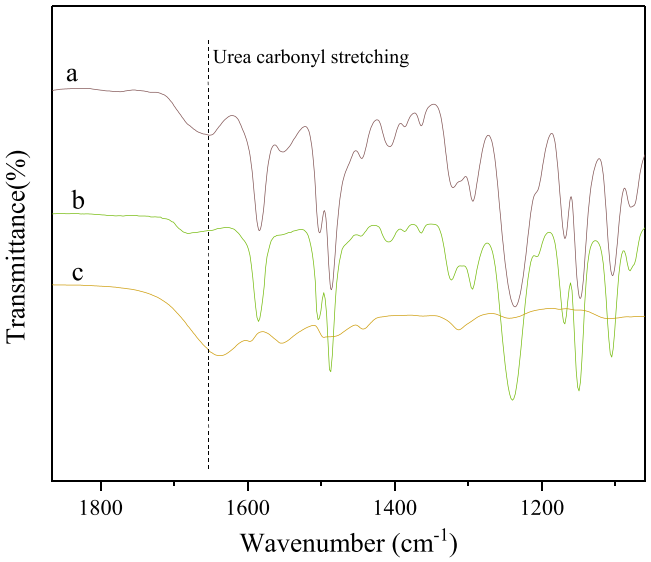

Fig. 8. FTIR spectra between 1000 and 2000 cm^{-1} of (a) fresh M10, (b) M10 after soaking 24 h in 0.64 M KOH and (c) neat UG20 additive. The band relative to C═O stretching of urea around 1660 cm^{-1} is highlighted.

If we focus our attention on the broad band around 1660 cm^{-1}, characteristic of C═O stretching of urea in neat UG20 (c), and compare the M10 before (a) and after soaking in KOH solution (b), we cannot find a great difference, though one could guess a slight displacement of this band towards higher wavenumbers for the sample submitted to the alkaline environment. This could be indicative of some hydrolysis of urea bond in this strong alkaline conditions. However, no clear conclusions could be drawn from this experiment. For this reason, we decided to check the stability of additivated M10 by ^{1}H NMR.

Fig. 9 shows the ^{1}H NMR spectra of M10 samples, as-prepared (red trace), after treatment in 0.64 M KOH solution followed by washing in water (green trace), and after treatment in water for 24 h (blue trace). In more detail, the region between 6.8 and 8.6 ppm, corresponding to the aromatic protons, is shown. Thanks to the comparison with the ^{1}H NMR spectra of UG20 additive alone and M0 sample, we could assign the regions 7.2–7.4, 7.5–7.65 and 8.05–8.35 to the signals from PSF protons, while the other ones were attributed to UG20 protons. No apparent changes in the additive signals could be evidenced after soaking in 0.64 M KOH for 24 h, which qualitatively suggested UG20 stability under this treatment conditions. Indeed, upon hydrolysis of urea and subsequent membrane washing, the originally grafted groups as well as the hydrolized UG20 should be washed out of the membrane and the amount of UG20 protons versus PSF protons should decrease in the ^{1}H NMR spectrum. In the three samples, quantification of the additive signals was performed by comparing the integration of the additive signals between 8.06 and 7.82 ppm with the integral of the singlet at 1.88 ppm, characteristic of PSF methyl group (Fig. S8). The ratio between the additive and the reference PSF areas gave the same value in all cases, within the experimental sensitivity: thus, no additive hydrolysis could be detected in the membrane under the tested conditions. In addition, one should take into account that stability was tested in such harsh conditions as completely soaking M10 in the capture solution while, in the CO_2 capture device, only the membrane bottom surface is in contact with it. Therefore, we could reasonably conclude that the membranes containing the additive are expected to exhibit good stability in service.

3.3. Mechanical characterization

Table 3 shows the tensile modulus, strain at break and ultimate strength of M0-M10 membranes; their glass transition temperatures

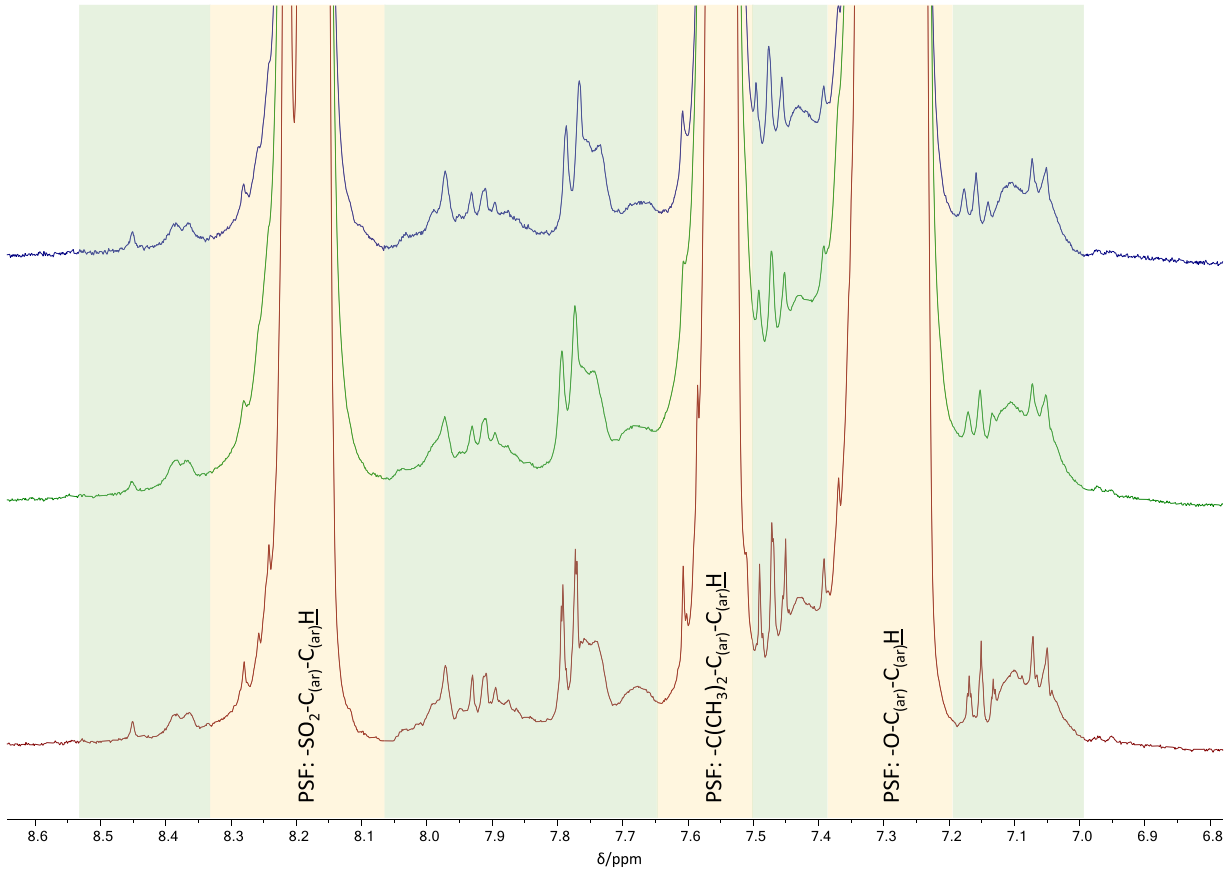

Fig. 9. Stacked ^{1}H NMR spectra (in DMF-d6, 400 MHz) between 6.8 and 8.7 ppm of M10 samples: as-prepared (red), after treatment 24 h in 0.64 M KOH solution and following washing (green) and after treatment in water (blue). Green- and yellow-shaded areas indicate the regions of additive (multiplets due to complex substitution patterns) and polysulfone (assigned) signals, respectively.

Table 3
Mechanical properties and glass transition temperatures of M0-M10 membranes.

Membrane	E (MPa)	Ultimate strength (MPa)	Strain at break (%)	Tg_d [a] (°C)	Tg_{NMP} [b] (°C)
M0	372 ± 64	3.0 ± 0.7	5.0 ± 1.3	178 ± 1	112 ± 2
M2	304 ± 30	2.8 ± 1.4	5.8 ± 2.0	171 ± 1	105 ± 1
M5	261 ± 27	2.0 ± 0.5	5.8 ± 1.2	139 ± 2	116 ± 1
M10	221 ± 31	1.7 ± 0.3	6.4 ± 1.4	133 ± 2	120 ± 3

[a] After 24 h washing in water and drying;
[b] after 30 min washing in water and drying.

after 24 h (Tg_d) and 30 min (Tg_{NMP}) washing and subsequent drying are also reported.

Table 3 shows that the presence of the additive has a plasticizing effect, as demonstrated by the 40% decrease of tensile modulus and 43% of tensile strength going from M0 to M10; moreover, the strain at break increased 28% with UG20 content, thus indicating a more plastic deformation. This suggested increased mobility of polymeric chains, which could be favorable to gas permeation. On the other hand, one should observe that the differences in porosity do not seem to affect the mechanical behavior, despite macrovoids and pores could act as weak points under an applied force [42]. Conversely, in our case the plasticizing effect of the additive seems to predominate over the porosity decrease going from M0 to M10. As a further evidence, as previously mentioned in Section3.1, if one compares the glass transition temperatures of the membranes after 30 min (Tg_{NMP}) and 24 h washing (Tg_d), lower values are found in the former case (Table 3). This also confirms the presence of residual NMP which acts as a plasticizer: thus, prolonged washing is necessary in order to completely remove residual NMP after phase inversion precipitation.

Fig. 10 displays the dielectric relaxation spectra of M0, M2 and M10 samples in terms of the loss factor (ε'') at 1 Hz of frequency in the temperature interval of − 150–250 °C.

Three complex relaxation zones ϒ, β and α, with increasing temperature order are observed, corresponding to molecular motions of both polysulfone and the modified hyperbranched polyethylene imine UG20. The loss factor is higher for the M2 and M10 membranes than M0, which would indicate a greater mobility of the molecular chains of the mixed membranes. This suggests that the additive imposes fewer restrictions on molecular movement by increasing the number of chains that can move, therefore facilitating the ability of the membrane to diffuse CO_2 [43–45]. The relaxation zone γ appears at low temperatures between − 150 °C and 50 °C, and the loss factor is independent of the additive concentration. At higher temperatures, between 120 °C and 250 °C, the most prominent relaxations are αPEI, αPSU, in increasing order of temperature: they arise from the motion of the main chains of PSU and PEI, respectively. The temperature of αPSU relaxation peak around 210 °C slightly decreases with the concentration of additive, whereas the most significant differences are observed in the αPEI relaxation. The temperature of this relaxation increases with the concentration of additive, being equal to 120 °C and 150 °C for M2 and M10, respectively. These first results confirm the plasticizing effect of UG20 as determined by mechanical tests and DSC. However, a more detailed analysis of the dielectric spectra of these membranes has been

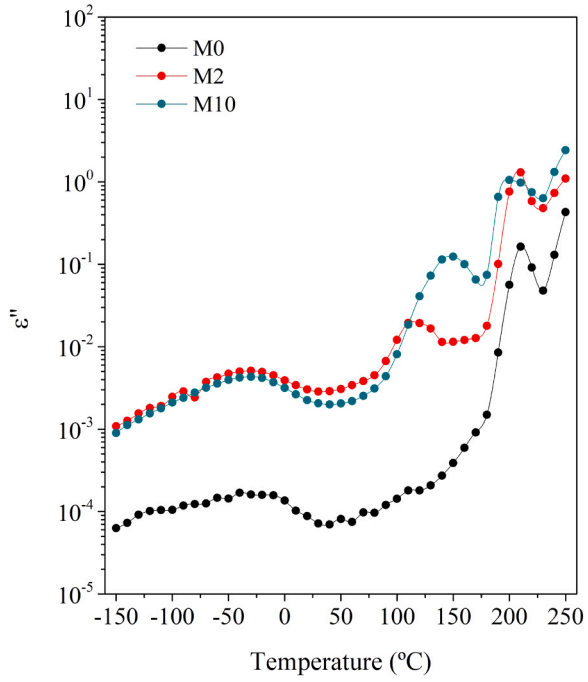

Fig. 10. Loss factor (ε'') versus temperature at 1 Hz of frequency for M0, M2 and M10 membranes.

performed and it is the object of a forthcoming paper [46].

3.4. CO_2 capture performance

Fig. 11 shows the solubility of CO_2 in M0-M10 membranes. As expected, CO_2 solubility increases with UG20 content, according to the high affinity of the additive to carbon dioxide due to the presence of basic nitrogen atoms which can favorably interact with this molecule. The grafting reaction performed on Lupasol G20 partially reduces the amount of amine nitrogen atoms available for carbon dioxide capture. Nevertheless, UG20 additive is expected to exhibit higher CO_2 solubility with respect to the previously reported mG20 additive [30]: indeed, the reaction between Lupasol G20 and phenyl isocyanate (Scheme 3) leads to the formation of urea groups, while amides are formed in the case of reaction with benzoyl chloride (mG20). This means that, as regards the grafted groups, UG20 contains double amount of nitrogen atoms than mG20; in addition, urea nitrogen atoms are expected to have more affinity to CO_2 than the amide ones. Therefore, higher carbon dioxide solubility can be expected in the UG20 containing membranes when comparable amounts of additive are considered.

We performed permeability tests to calculate the mass transfer coefficients *k*, for the M0-M10 membranes series. The selectivity of CO_2 transfer was determined versus N_2. The results are shown in Fig. 12. The inset in Fig. 12 depicts carbon dioxide selectivity, calculated as the ratio of their respective mass transfer coefficients.

As shown in Fig. 12, in general k for carbon dioxide increases after addition of UG20, while no clear trend can be found in the case of nitrogen. Selectivity to carbon dioxide versus nitrogen (Inset of Fig. 12) is approximately 1 in the case of M0 and its increasing with the increase of the UG20 content. This suggests that the permeation of these gases does not only depend on the relationship between membrane pores and molecular size of gases, but also on the chemical composition and the capability of the compounds to physically adsorb the gas and increase its local concentration. In particular, it must be noticed that the mass transfer coefficient for CO_2 ratio reaches a maximum in correspondence to M5 sample and then decreases for M10, though, it still exhibits a higher value than M2. However, CO_2 selectivity exhibits the highest value for M10 sample. In order to explain this behavior, we should consider that different factors are involved in the gas transport of these systems.

In general, when polymeric membranes are non-porous the gas permeation through them can be described by the solution-diffusion mechanism [47]. The membranes under investigation are asymmetric and present several ranges of pore size (Fig. 6 and Fig.S4), lying in macro-, meso- and microporosity range. Selectivity will be therefore determined mainly by the denser layer, whose thickness, in the case of

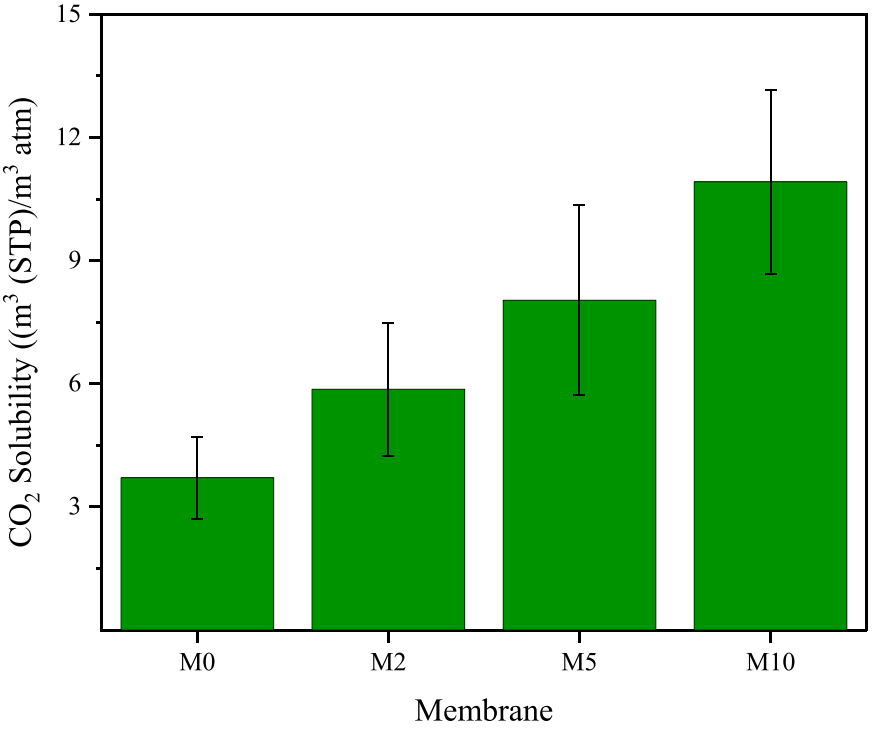

Fig. 11. CO_2 solubility in M0-M10 membranes determined by the pressure decay method at 2 bar.

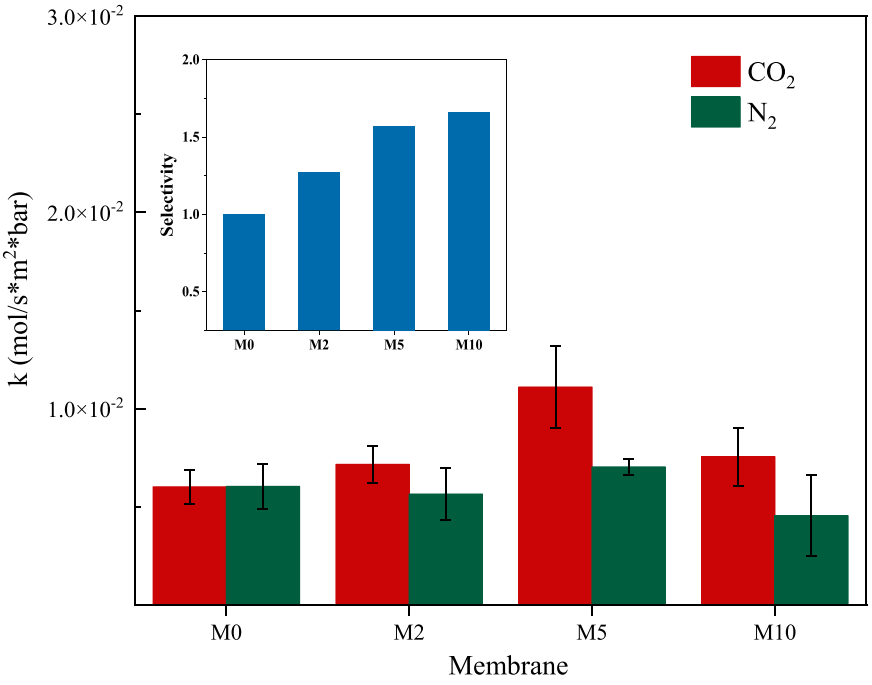

Fig. 12. Mass transfer coefficient k as calculated from CO_2 (red bar) and N_2 (green bar) permeation through M0-M10 membranes. In the inset the corresponding selectivities calculated as kCO_2/kN_2 are shown.

M0-M10 membranes, could not be clearly determined. The selectivity can be split into a solubility selectivity and a diffusivity selectivity: therefore, it can be ascribed to a difference in both properties [48]. When we consider these two factors, the former depends on the gas affinity to the membrane material and its condensability, while the latter can be ascribed to the free volume and random motion of the polymeric chains. Typically, diffusivity increases with decreasing the gaseous molecule kinetic diameter and increasing the polymer free volume. Since the CO_2 and N_2 kinetic diameters are 0.330 nm and 0.364 nm, respectively, the former is favored as regards diffusivity selectivity; moreover, gas condensability increases with its critical temperature, which is 304.1 K in the case of CO_2 and 126.2 K for N_2 [49]. Summing up, in general permeability of CO_2 is favored over N_2. On the other hand, we found that the mass transfer coefficient of CO_2 increases considerably upon addition of UG20 as expected, since CO_2 solubility increases (Fig. 11); nevertheless, it reaches a maximum in correspondence to M5 and then slightly decreases. This trend suggests that two factors, acting in opposite directions, contribute to CO_2 permeation and reach the best balance in M5 sample. As for solubility, it increases with UG20 amount: so, it should contribute to increasing permeability of M10 over M5. This suggests that the explanation of the observed experimental trend of the mass transfer coefficients needs to be sought in the diffusivity factor. A plasticizing effect of UG20 additive has been demonstrated by both DSC and Dielectric data, which would indicate a greater mobility of the molecular chains of the additivated membranes. This, in turn, is expected to improve diffusivity. Nevertheless, BET analysis showed that porosity is strongly reduced on UG20 addition and exhibits the lowest value in the case of M10. As a final remark, we should also take into account that, given the strong asymmetry of these membranes, the thickness of the dense layer could not be exactly determined and could be much higher in the case of M10, thus improving membrane resistance to permeant diffusion.

Obtained membranes were further used in a cross-flow contactor where the direct air capture was studied with use of potassium hydroxide aqueous solution as absorbent. Fig. 13 shows the results in terms of carbon dioxide flux versus absorbent flow rate.

From Fig. 13, one can see that CO_2 absorption from ambient air exhibits similar values for all the membranes under investigation at

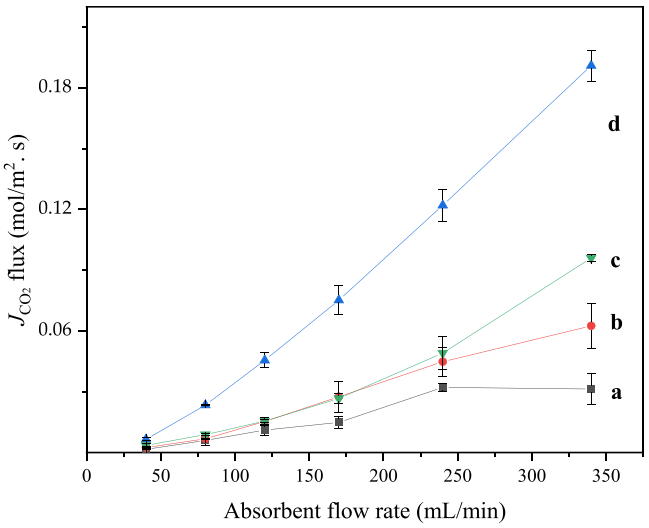

Fig. 13. CO_2 absorption flux into M0–M10 membranes in direct air capture tests as a function of liquid absorbent (0.64 M KOH) flow rate: (a) M0; (b) M2; (c) M10; (d) M5.

35 mL/min that is the lowest absorbent flow rate. The mass transfer process in the gas/liquid membrane contactors is rules by three resistances: liquid side, gas side and membrane mass transfer resistances [50,51]. In our case, the effect of gas side resistance was neglected, since ambient air we used as CO_2 source: as a consequence, CO2 concentration was stable and no pressure was applied in all our experiments. So, the total mass transfer resistance at low liquid flow rate is mainly affected by the liquid side resistance. This can explain very similar gas absorption flux at low liquid absorbent flow rate for M0-M10 membranes, as shown in Fig. 13. However, when the absorbent flow rate was increased (120–340 mL/min), we found remarkable differences that can be explained in terms of the different UG20 additive content; in more detail, the behavior of the membrane with 5% additive amount (M5) is the most efficient: that is, UG20 amount higher than 5% does not

improve the membrane performance any more, though it gives better CO_2 capture than neat PSF (M0) in all cases, and then M2 at high liquid absorbent flow rate. In general, by increasing the liquid flow rate on can decrease the liquid side mass transfer resistance and at a certain flow rate, the mass flux will be mainly affected by the membrane resistance. At this point, absorption flux will reach plateau with further increase if the liquid flow rate. In the present flow ranges, this is applies to membrane M0. As for the additivated membranes, the trend of CO_2 absorption flux is the same as the one we found for mass transfer coefficient, i.e. M5 exhibits the best performance; in all cases, M2-M10 outperform the results of the PSF membranes previously reported, which contained less stable amide-functionalized additive, namely mG20 [30]. Indeed, on comparing the performance of M2-M10 membranes in the contactor, with the analogous ones additivated with mG20 [30], in general higher values of the flux were found. The optimum CO_2 absorption flux achieved with M5 was above 150 mmol(CO_2)/(m^2·s), largely surpassing previous results obtained for mG20, which maximum reached value was 4.5 mmol(CO_2)/(m^2·s). These very promising results can be ascribed to higher values of CO_2 permeability, in combination with lower water and KOH uptake, which can determine lower pore clogging, and higher stability of the additive to the alkaline environment.

On the other hand, we should also consider the increase in membranes' wettability and water uptake as a consequence of higher content of UG20, which can favor the penetration of KOH solution into the membrane, thus provoking pores obstruction and negatively affecting gas diffusivity during extended hours of use. At the bottom side of the membranes in the contactor, where CO_2 as a permeant gets in touch with the aqueous solution of KOH, the absorption reaction produces an aqueous solution of K_2CO_3; on the other hand, when CO_2 is in excess, the undesired production of more insoluble $KHCO_3$ can occur. Consequently, pores may be clogged and the pore volume decreases. Indeed, Fig. 14a shows the ESEM image of bottom surface of M10 after CO_2 absorption test, which puts into evidence very nice hexagonal crystals layered onto the polymeric surface. By means of XRD and EDX analyses (Figs. 14b and 14c, respectively), these crystals could be identified as $KHCO_3$.

Furthermore, it is of fundamental importance to compare the performance of M2-M10 systems to stomatal CO_2 assimilation efficiency. In order to do this, the results of CO_2 flux generated in the laboratory need to be recalculated from Eq. 6 according to the Eq. (7).

$$J = \frac{n}{A \cdot t} \tag{7}$$

where n is moles of CO_2, A is the membrane area in m^2 and t is experimental time in s.

The calculated CO_2 assimilation rates versus absorbent flow rate are reported in Fig. S9. The assimilation rates of all prepared membranes range between 67 and 938 μmol/(m^2·s) (Fig. S9), which remarkably overcome the assimilation rate reported for natural stomata, which is typically in the range 15–40 μmol/(m^2·s) depending on the plant species used for investigation [15,52,53]. These values also demonstrate that the presence of UG20 additive can improve the performance with respect to the previously reported artificial membrane contactors based on PSF [16], which CO_2 uptake ranged between 27.7 and 284.2 μmol/(m^2·s). In addition, the trend demonstrated in Fig. S9 suggests that, while in M0 and M2 membranes the assimilation rate vs. absorbent flow rate reaches a plateau, in the case of M5 and M10 membranes, the increase of absorbent flow rate could even further improve CO_2 uptake.

For sake of comparison, we also considered the estimation of carbon dioxide capture from air in an industrial module described by Holmes et al. [54,55]. These authors reported the design of an industrial module based on a slab and at least one liquid source, designed as multiple packed towers. In this case, CO_2 uptake was predicted in the range 14–19 mmol/(m^2·s); however, one should remember that this result is an estimation based on the use of commercial packings with 1 or 2 M NaOH or KOH aqueous solutions in laboratory-scale tests.

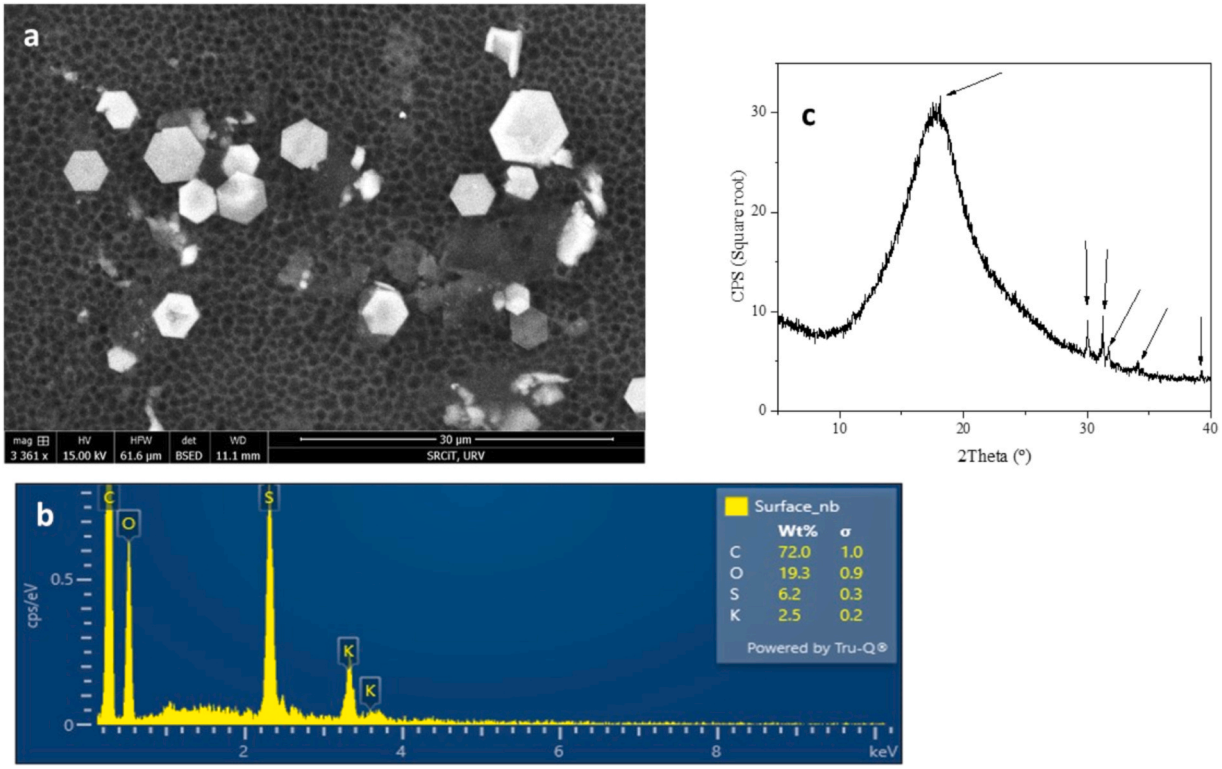

Fig. 14. (a) ESEM image of M10 bottom surface; (b) EDX analysis of bottom surface observed by ESEM; (c) XRD pattern of M10 bottom surface; the arrows evidence the crystalline peaks which overlap with the pattern of crystalline $KHCO_3$.

4. Conclusions

We investigated the behavior of asymmetric Polysulfone membranes prepared via phase-inversion precipitation with the addition of UG20 additive, based on hyperbranched Lupasol G20 grafted with phenyl isocyanate. This modification strategy rendered the additive more hydrophobic and hence more resistant to leaching and degradation in contact with aqueous alkaline sorbents. Membranes were prepared by blending PSF with UG20 amount between 2 and 10 wt.10%, with the aim to increase their ability for carbon dioxide capture at ambient pressure. In all cases the resulting morphology showed finger-like macropores together with meso- and micropores as well as a dense layer. However, porosity decreased on increasing the additive content, probably as a consequence of delayed demixing during phase inversion precipitation. The presence of the additive determined an increase of water and KOH uptake with respect to neat PSF. However, no degradation upon 24 h soaking in KOH solution could be detected neither by FTIR nor ^{1}H NMR. Mechanical, thermal and dielectric analysis showed a plasticizing effect of the additive, which could favor gas permeation. On the other hand, CO_2 solubility was remarkably increased as a consequence of UG20 addition. Nevertheless, the CO_2 mass transfer coefficient improved up to 5% additive, while was reduced in 10% UG20 sample, probably due to the porosity decrease which acted in reverse to the increased solubility. Finally, when we evaluated the performance of obtained membranes in the direct air capturing device, we found a remarkable improvement in comparison with neat PSF; the capture behavior showed the same trend as the mass transfer coefficient, i.e. the best performance was obtained with use of 5% UG20. In general, the use of UG20 as an additive determined better characteristics in terms of CO_2 permeability and capture when compared with the additive mG20 previously reported. The enhancement in hydrophobicity and chemical stability of the urea-modified additive UG20 as compared to the amide-functionalized analogue mG20, are key for the high direct air capture efficiency and robustness observed. CO_2 assimilation rate was found remarkably higher than in the natural stomata of plant leaves and in the PSF-based module previously reported in the literature.

Funding

This work is part of Grants PID2020–116322RB-C32 and PID2020–116322RB-C31 funded by the Spanish Research State Agency (Agencia Estatal de Investigación, AEI/10.13039/501100011033). A.P. thanks the Spanish Ministry of Science and Innovation, the Spanish Research State Agency, (MCIN/AEI/10.13039/501100011033) and the European Social Fund for a "Ramón y Cajal" contract (RYC-2017–22849). This project has received funding from the European Union's Horizon 2020 research and innovation programme under the Marie Skłodowska-Curie grant agreement No. 713679 and from the Universitat Rovira i Virgili (URV).

Declaration of Competing Interest

The authors declare that they have no known competing financial interests or personal relationships that could have appeared to influence the work reported in this paper.

Data availability

Data will be made available on request.

Acknowledgements

The authors are grateful to Dr. Anton Dafinov for helpful discussion on porosity analyses.

Appendix A. Supporting information

Supplementary data associated with this article can be found in the online version at doi:10.1016/j.jcou.2023.102629.

References

[1] H. Herzog, B. Eliasson, O. Kaarstad, Capturing greenhouse gases, Sci. Am. 182 (2000) 72–79.
[2] M. Kharseh, L. Altorkmany, How global warming and building envelope will change buildings energy use in central Europe, Appl. Energy 97 (2012) 999–1004.
[3] P.A. Arias, N. Bellouin, E. Coppola, R.G. Jones, G. Krinner, J. Marotzke, V. Naik, M. D. Palmer, G.K. Plattner, J. Rogelj, e.t. al., Climate Change 2021: the Physical Science Basis, Contrib. Work. Group I Sixth Assess. Rep. Intergov. Panel Clim. Change (2021) 33–144.
[4] IEA, World Energy Outlook 2022, IEA, Paris ⟨https://www.iea.org/reports/world-energy-outlook-2022⟩ (2022).
[5] S.D. Bazhenov, A.V. Bildyukevich, A.V. Volkov, Gas-liquid hollow fiber membrane contactors for different applications, Fibers 6 (4) (2018) 76.
[6] S. Zhao, P.H.M. Feron, L. Deng, E. Favre, E. Chabanon, S. Yan, J. Hou, V. Chen, H. Qi, Status and progress of membrane contactors in post-combustion carbon capture: a state-of-the-art review of new developments, J. Membr. Sci. 511 (2016) 180–206, https://doi.org/10.1016/j.memsci.2016.03.051.
[7] A.B. Rao, E.S. Rubin, A. Technical, Economic, and environmental assessment of amine-based CO_2 capture technology for power plant greenhouse gas control, Environ. Sci. Technol. 36 (2002) 4467–4475.
[8] M. Rahbari-Sisakht, A.F. Ismail, D. Rana, T. Matsuura, D. Emadzadeh, Carbon dioxide stripping from water through porous polysulfone hollow fiber membrane contactor, Sep. Purif. Technol. 108 (2013) 119–123.
[9] M. Rahbari-Sisakht, A.F. Ismail, D. Rana, T. Matsuura, Effect of novel surface modifying macromolecules on morphology and performance of polysulfone hollow fiber membrane contactor for CO_2 absorption, Sep. Purif. Technol. 99 (2012) 61–68.
[10] A. Witek-Krowiak, A. Dawiec, S. Modelski, D. Podstawczyk, Carbon dioxide removal in a membrane contactor-selection of absorptive liquid/membrane system, Int. J. Chem. Eng. Appl. 3 (2012) 391–395.
[11] S. Hafeez, T. Safdar, E. Pallari, G. Manos, E. Aristodemou, Z. Zhang, S.M. Al-Salem, A. Constantinou, CO_2 capture using membrane contactors: a systematic literature review, Front. Chem. Sci. Eng. 15 (4) (2021) 720–754, https://doi.org/10.1007/s11705-020-1992-z.
[12] C.A. Scholes, G.Q. Chen, G.W. Stevens, S.E. Kentish, Journal of membrane science: plasticization of ultra-thin polysulfone membranes by carbon dioxide, Cell. Polym. 29 (1) (2010) 71.
[13] The Royal Society. Geoengineering the climate: science, governance and uncertainty, https://royalsociety.org/topics-policy/publications/2009/geoengineering-climate/ (2009).
[14] K.Z. House, A.C. Baclig, M. Ranjan, E.Av Nierop, J. Wilcox, H.J. Herzog, Economic and energetic analysis of capturing CO_2 from ambient air, Proc. Natl. Acad. Sci. USA 108 (51) (2011) 20428–20433, https://doi.org/10.1073/pnas.1012253108.
[15] A.R. Hemsley, I. Poole, The Evolution of Plant Physiology: From Whole Plants to Ecosystems, Linnean Society of London (2004).
[16] A. Nogalska, M. Ammendola, B. Tylkowski, V. Ambrogi, R. Garcia-Valls, Ambient CO_2 adsorption via membrane contactors - Value of assimilation from air as nature stomata, J. Membr. Sci. 546 (2018) 41–49.
[17] J. Martinez Luscher, F. Morales, S. Delrot, J. Aguirreolea, E. Gomes, I. Pascual, G. Hilbert, Climate change conditions (elevated CO_2 and temperature) and UV-B radiation affect grapevine (Vitis vinifera cv. Tempranillo) leaf carbon assimilation, altering fruit ripening rates, Plant Sci. 236 (2015) 168–176, https://doi.org/10.1016/j.plantsci.2015.04.001.
[18] M. Afsari, S. Kheyrieh, M. Asghari, Application and modification of polysulfone membranes in wastewater treatment - A review, Rev. Chem. Eng. (2017), https://doi.org/10.1515/revce-2017-0011/html.
[19] D.F. Sanders, Z.P. Smith, R. Guo, L.M. Robeson, J.E. McGrath, D.R. Paul, B. D. Freeman, Energy-efficient polymeric gas separation membranes for a sustainable future: A review, Polymer 54 (18) (2013) 4729–4761, https://doi.org/10.1016/j.polymer.2013.05.075.
[20] S. Kheirieh, M. Asghari, M. Afsari, Application and modification of polysulfone membranes, Rev. Chem. Eng. 34 (5) (2018) 657–693, https://doi.org/10.1515/revce-2017-0011.
[21] E. Kianfar, V. Pirouzfar, H. Sakhaeinia, An experimental study on absorption/stripping CO_2 using mono-ethanol amine hollow fiber membrane contactor, J. Taiwan Inst. Chem. Eng. 80 (2017) 954–962, https://doi.org/10.1016/j.jtice.2017.08.017.
[22] I.M. Bernhardsen, H.K. Knuutila, A review of potential amine solvents for CO_2 absorption process: Absorption capacity, cyclic capacity and pKa, Int. J. Greenh. Gas. Control 61 (2017) 27–48, https://doi.org/10.1016/j.ijggc.2017.03.021.
[23] H. Yamada, Amine-based capture of CO_2 for utilization and storage, Polym. J. 53 (1) (2021) 93–102, https://doi.org/10.1038/s41428-020-00400-y.
[24] F.A. Chowdhury, H. Okabe, H. Yamada, M. Onoda, Y. Fujioka, Synthesis and selection of hindered new amine absorbents for CO_2 capture, Energy Procedia 4 (2011) 201–208, https://doi.org/10.1016/j.egypro.2011.01.042.
[25] F. Bougie, M.C. Iliuta, Sterically Hindered Amine-Based Absorbents for the Removal of CO_2 from Gas Streams, J. Chem. Eng. Data 57 (3) (2012) 635–669, https://doi.org/10.1021/je200731v.

[26] H. Yang, Z. Xu, M. Fan, R. Gupta, R.B. Slimane, A.E. Bland, I. Wright, Progress in carbon dioxide separation and capture: a review, J. Environ. Sci. (China) 20 (1) (2008) 14–27.
[27] B.P. Spigarelli, S.K. Kawatra, Opportunities and challenges in carbon dioxide capture, J. CO_2 Util. 1 (2013) 69–87, https://doi.org/10.1016/j.jcou.2013.03.002.
[28] X. Shen, H. Du, R.H. Mullins, R.R. Kommalapati, Polyethylenimine Applications in Carbon Dioxide Capture and Separation: From Theoretical Study to Experimental Work, Energy Technol. 5 (6) (2017) 822–833, https://doi.org/10.1002/ente.201600694.
[29] S. Satyapal, T. Filburn, J. Trela, J. Strange, Performance and Properties of a Solid Amine Sorbent for Carbon Dioxide Removal in Space Life Support Applications, Energy Fuels 15 (2) (2001) 250–255, https://doi.org/10.1021/ef0002391.
[30] A. Zare, L. Perna, A. Nogalska, V. Ambrogi, P. Cerruti, B. Tylkowski, R. García-Valls, M. Giamberini, Polymer Blends for Improved CO_2 Capture Membranes, Polymers 11 (10) (2019) 1662, https://doi.org/10.3390/polym11101662.
[31] H. Marvaniya, K. Modi, D.D.J. Sen, Greener reactions under solvent free conditions, Int. J. Drug Dev. Res. 3 (2011) 34–43.
[32] S.-H. Lin, K.-L. Tung, H.-W. Chang, K.-R. Lee, Influence of fluorocarbon flat-membrane hydrophobicity on carbon dioxide recovery, Chemosphere 75 (10) (2009) 1410–1416, https://doi.org/10.1016/j.chemosphere.2009.02.027.
[33] S.-H. Yeon, B. Sea, Y.-I. Park, K.-H. Lee, Determination of Mass Transfer Rates in PVDF and PTFE Hollow Fiber Membranes for CO_2 Absorption, Sep. Sci. Technol. 38 (2) (2003) 271–293, https://doi.org/10.1081/ss-120016575.
[34] J.M. Morancho, X. Fernández-Francos, C. Acebo, X. Ramis, J.M. Salla, À. Serra, Thermal curing of an epoxy-anhydride system modified with hyperbranched poly (ethylene imine)s with different terminal groups, J. Therm. Anal. Calorim. 127 (1) (2017) 645–654, https://doi.org/10.1007/s10973-016-5376-z.
[35] P. van de Witte, P.J. Dijkstra, J.W.A. van den Berg, J. Feijen, Phase separation processes in polymer solutions in relation to membrane formation, J. Membr. Sci. 117 (1) (1996) 1–31, https://doi.org/10.1016/0376-7388(96)00088-9.
[36] P.S.T. Machado, A.C. Habert, C.P. Borges, Membrane formation mechanism based on precipitation kinetics and membrane morphology: flat and hollow fiber polysulfone membranes, J. Membr. Sci. 155 (2) (1999) 171–183, https://doi.org/10.1016/S0376-7388(98)00266-X.
[37] D. Li, T.-S. Chung, J. Ren, R. Wang, Thickness Dependence of Macrovoid Evolution in Wet Phase-Inversion Asymmetric Membranes, Ind. Eng. Chem. Res. 43 (6) (2004) 1553–1556, https://doi.org/10.1021/ie034264g.
[38] P.A. Webb, C. Orr, Analytical Methods in Fine Particle Technology, Micromeritics Instrument (1997).
[39] C.Y. Feng, K.C. Khulbe, T. Matsuura, A.F. Ismail, Recent progresses in polymeric hollow fiber membrane preparation, characterization and applications, Sep. Purif. Technol. 111 (2013) 43–71, https://doi.org/10.1016/j.seppur.2013.03.017.
[40] P. Vaughan, J. Donohue, The structure of urea. Interatomic distances and resonance in urea and related compounds, Acta Crystallogr. 5 (1952) 530.
[41] E.A. Campo, 1 - Polymeric Materials and Properties, in: E.A. Campo (Ed.), Selection of Polymeric Materials, William Andrew Publishing, Norwich, NY, 2008, pp. 1–39, https://doi.org/10.1016/B978-081551551-7.50003-6.
[42] H.-A. Tsai, D.-H. Huang, R.-C. Ruaan, J.-Y. Lai, Mechanical Properties of Asymmetric Polysulfone Membranes Containing Surfactant as Additives, Ind. Eng. Chem. Res. 40 (25) (2001) 5917–5922, https://doi.org/10.1021/ie010026e.
[43] S. Bano, S.R. Tariq, T. Anjum, M. Najam, M. Usman, M. Yasin, H. Shafi, A.L. Khan, Development of highly permselective Mixed Matrix Membranes comprising of polyimide and Ln-MOF for CO_2 capture, Chemosphere 307 (2022), 136051.
[44] R.R. Wanderley, D.D.D. Pinto, H.K. Knuutila, From hybrid solvents to water-lean solvents – A critical and historical review, Sep. Purif. Technol. 260 (2021), 118193, https://doi.org/10.1016/j.seppur.2020.118193.
[45] M. Muschi, S. Devautour-Vinot, D. Aureau, N. Heymans, S. Sene, R. Emmerich, A. Ploumistos, A. Geneste, N. Steunou, G. Patriarche, G. De Weireld, C. Serre, Metal–organic framework/graphene oxide composites for CO_2 capture by microwave swing adsorption, J. Mater. Chem. A 9 (22) (2021) 13135–13142, https://doi.org/10.1039/d0ta12215g.
[46] B. Pascual-Jose, A. Zare, M. Giamberini, J.A. Reina, A. Ribes-Greus, Dielectric analysis of blended Polysulfone/Polyethyleneimine membrane contactors for CO_2 capture, Macromol. Rapid Comun. submitted.
[47] D. Paul, Y. Yampol'skii, Polymeric gas separation membranes, CRC Press, Baton rouge, 1994.
[48] J. Wijmans, R. Baker, The solution-diffusion model: A review, J. Membr. Sci. 107 (1) (1995) 1–21.
[49] C.A. Scholes, S.E. Kentish, G.W. Stevens, Carbon Dioxide Separation through Polymeric Membrane Systems for Flue Gas Applications, Recent Pat. Chem. Eng. 1 (2008) 52–66.
[50] A. Gabelman, S.-T. Hwang, Hollow fiber membrane contactors, J. Membr. Sci. 159 (1–2) (1999) 61–106, https://doi.org/10.1016/S0376-7388(99)00040-X.
[51] G. Bakeri, A.F. Ismail, M.R. DashtArzhandi, T. Matsuura, Porous PES and PEI hollow fiber membranes in gas-liquid contacting process - A comparative study, J. Membr. Sci. 475 (2015) 57–64.
[52] W. Tezara, V.J. Mitchell, S.D. Driscoll, D.W. Lawlor, Water stress inhibits plant photosynthesis by decreasing coupling factor and ATP, Nature 401 (6756) (1999) 914–917, https://doi.org/10.1038/44842.
[53] K. Radoglou, Environmental control of CO_2 assimilation rates and stomatal conductance in five oak species growing under field conditions in Greece., Annales des sciences forestières, INRA/EDP Sci. 53 (2–3) (1996) 269–278.
[54] G. Holmes, D.W. Keith, An air-liquid contactor for large-scale capture of CO_2 from air, Philos. Trans. R. Soc. A. 370 (2012) 4380–4403, https://doi.org/10.1098/rsta.2012.0137.
[55] D. Keith, M. Mahmoudkhani, A. Biglioli, B. Hart, K. Heidel, M. Foniok, CARBON DIOXIDE CAPTURE METHOD AND FACILITY, in: C.E.L. Partnership (Ed.) Carbon Engineering Limited Partnership, USA, 2015.